ISSN 2004-2965 Energy Proceedings, Vol. 20, 2021

International Conference on Applied Energy 2021
Nov. 29 - Dec. 5, 2021, Thailand/Virtual
Paper ID:664

Surrogate Modelling for Battery State-of-Charge Estimation in Electric Vehicles Based on Pseudo-2-Dimensional Model and Gradient Boosting Machines

Min Hua [1], Quan Zhou[1], Chongming Wang[2], Cetengfei Zhang[1], Bin Shuai[1], Hongming Xu [1*]
1 Department of Mechanical Engineering, University of Birmingham, B15 2TT, UK (*Corresponding Author)
2 Institute for Future Transport and Cities, Coventry University, CV1 5FB, UK

ABSTRACT

Lithium-ion batteries are the main power source of electric vehicles (EVs). Prediction of battery State-of-Charge (SoC) for EV is important but challenging because battery SoC cannot be directly measured through onboard sensors. This paper proposes a surrogate model for battery SoC evaluation based on a Pseudo 2-Dimensional (P2D) model, offering increased physical insight and predictability than the conventional Resistance-Capacitor (RC) model in a computationally efficient way. By simulating battery performance under different cycles using COMSOL, the proposed P2D model demonstrates its strong representation capability quantified by Root Mean Square Error (RMSE), which can be controlled below 0.03 under all studied conditions while providing physical and analytical characteristics in battery operation. Furthermore, based on the simulated data from the P2D model, the proposed surrogate modeling using Gradient Boosting Machines (GBMs) is proposed to build the recurrent model for the voltage and SoC prediction using previous voltages. The results from GBR with Root Mean Square Error (RMSE) 0.0387 are close to training data with RMSE 0.0258.

Keywords: Lithium-ion Battery, Surrogate Battery Modelling, State-of-Charge, Gradient Boosting Regression

1. INTRODUCTION

Thanks to the progress in advanced power battery technology, the blooming development of electric vehicles (EVs) effectively has achieved significant progress in energy saving and emission reduction in recent years [1][2]. Lithium-ion batteries (LIBs) with characteristics of high energy, low self-discharge rate and long cycle life, therefore, are widely considered as the most promising power sources for electrified vehicles [3]. It is indispensable to develop battery management systems (BMSs) that are important to coordinate the work of individual battery cells while maintaining their safety and health [4][5]. At the core of BMSs[6] are well-established battery models that are capable of predicting internal characteristics and electro-chemical dynamics of the battery during vehicle operation.

Generally, the internal characteristics and electro-chemical dynamics of LIBs are represented by 1) Equivalent Circuit Model (ECM), 2) Electrochemical Model (EM), 3) Electrochemical Impedance Spectrum Models, and 4) Data-driven Models [7]. Compared with the four types of LIB models above, the pseudo-two-dimensional (P2D) model is one of the most representative EMs that can offer increased physical insight and predictability[8]. If the model parameters are properly specified, the internal characteristics of LIBs could be accurately investigated by electrochemical simulation, which is important for the analysis of the decay and ageing mechanism of the LIBs [9].

Single-particle model is a simplified P2D model with two spherical particles[10]. It is built on two assumptions: 1) the insertion and extraction process of lithium-ions occurs on the spherical particles, and 2) the concentration and internal potential of the electrolyte are constant. However, the single-particle model cannot be directly used for vehicle application because these two assumptions are not suitable for the LIBs under high C-rate charging and discharging conditions. It is not suitable to serve many purposes such as estimation and life modelling of Li-ion batteries due to excessive simulation deviations. To overcome the problem, this paper proposes a P2D model with spherical particles

Selection and peer-review under responsibility of the scientific committee of the 13th Int. Conf. on Applied Energy (ICAE2021).
Copyright © 2021 ICAE

surrounded by the electrolyte using incorporating statistical learning methods. This work aims to improve the representation capability of the battery model for evaluation of battery State-of-Charge (SOC).

SOC estimation methods can be classified into 1) direct estimation methods, 2) filtering methods, and 3) data-driven methods [11]. Direct estimation methods estimate battery SOC by looking up the SOC-OCV table, and the fitness of open-circuit voltage (OCV) curves is essential for the direct methods. Filtering methods mainly adopt the Kalman filter to estimate the SOC by mapping the battery states with observation equations. However, it is tough to establish an accurate mathematical model of a battery with particular complexity and nonlinearity.

Data-driven methods based on statistical learning techniques, such as Neural Networks (NNs), Decision Trees (DTs), and Random Forests (RFs), Gradient Boosted Machines (GBMs), have been studied for SOC estimation [12]. And the data-driven methods cannot provide insight into detailed internal battery mechanisms because the internal reactions are regarded as a black-box, and these are employed to build functional relationships between input and output variables. However, the data-driven methods are also suffering the following issues. When adopting the NN method, it is easy to fall into the local optimum using gradient-based parameter tuning. It is hard for data-driven methods to balance optimality and computational efficiency[13]. DTs are established by creating sets of rules applied to new data of a similar format. RFs are the idea of ensembles and randomized such that each has the possibility of obtaining a different output for a given input, the results of which are combined using a weighted sum with different methods. Similarly, GBMs are ensembles of many DTs where the maximum depth is heavily limited such that the model generalizes more aggressively[14]. During distinct application cases, each algorithm can perform diversely in training time, accuracy, and execution time. In this paper, compared to DTs and RFs, GBMs with the ensemble of multiple weak and various predictors produce better generalizability.

When the amount of data is not enough, it is untoward for a data-driven scheme to make accurate predictions; on the contrary, when the amount of data is too large, the computational load increases exponentially, causing a significant reduction in computation efficiency. To overcome the drawbacks of the existing method, a GBMs based surrogate battery model producing numerous simulated data combined with the P2D model is proposed to emulate the Li-ion battery with physical characteristics. The work is conducted with two new contributions: 1) a simplified P2D model is developed based on the finite volume method, and it aims to balance the conflicting goals of model accuracy and computational efficiency, and 2) a gradient boosting machine is developed to enhance the representative capability of the P2D model for OCV and SOC prediction.

The remainder of the paper is organized as follows: the surrogate models from P2D models are described in Section 2. Implement simulation to validate the P2D model is introduced in Section 3. Section 4 introduces State-of-Charge estimation based on gradient boosting machine algorithm. Conclusions are drawn in Section 5.

2. SURROGATE MODELS FROM P2D MODELS

The pseudo-two-dimensional model (P2D) of a lithium-ion battery, describing the electrochemical behavior with internal Li-ions transfer process and external electron motion process, is illustrated in Fig.1. It has three main sections, i.e., the electrodes (negative n and positive p), the separator s, and the current collectors(a, z). The grain size of quasi-spherical active particles is in both electrodes. In this paper, active particles in the two electrodes are considered spherical. The diffusion and the migration of the Li-ions are performed through these active particles along their r-axises. Based on the porous electrode theory, the P2D model is built on a series of coupled nonlinear partial differential-algebraic equations (PDAEs), representing the conservation of mass and charge in the three sections of the Li-ion battery. The details of the P2D model are given below.

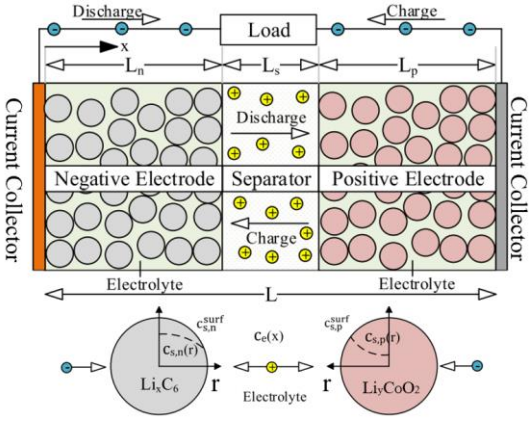

Fig. 1 Schematic of the P2D cell model[7]

2.1 Li-ion diffusion equation in the solid phase

Copyright © 2021 ICAE

Following Fick's second law [15], the Li-ions concentration, c, of the solid spherical particles of the positive (*p*) and negative (*n*) electrodes yields.

$$\frac{\partial c^s(r,t)}{\partial t} = \frac{1}{r^2}\frac{\partial}{\partial r}\left[r^2 D_p^s \frac{\partial c^s(r,t)}{\partial r} \right] \tag{1}$$

The initial condition and Newman boundary conditions are:

$$\left.\frac{\partial c^s(r,t)}{\partial r}\right|_{r=0} = 0 \tag{2}$$

$$-D_{eff}^s \left.\frac{\partial c^s(r,t)}{\partial r}\right|_{r=R_p} = j(x,t) \tag{3}$$

where D_p^s is the solid phase diffusion coefficient of the Li-ions within the solid particles("*eff*" suffixes represents effective values); $j(x,t)$ is the local volumetric transfer current density at position *x* and time *t* (j >0 represents discharge), and *r* is the radius of the all particles.

2.2 Potential equation in the solid phase

Based on Ohm's law, the potential distribution Φ_s in the solid phase is

$$\frac{\partial}{\partial x}\left[\sigma_{eff,i} \frac{\partial}{\partial x}\Phi_s(x,t) \right] = a_i F j(x,t) \tag{4}$$

Due to physical constraints, zero flux boundary conditions at the interface between electrodes and the separator are described as:

$$\left.\sigma_{eff,i}\frac{\partial}{\partial x}\Phi_s(x,t)\right|_{x=\hat{x}_0,\hat{x}_n} = -I_{app}(t) \tag{5}$$

$$\left.\sigma_{eff,i}\frac{\partial}{\partial x}\Phi_s(x,t)\right|_{x=\hat{x}_p,\hat{x}_s} = 0 \tag{6}$$

where $\sigma_{eff,i}$ is the effective solid-phase conductivity.

2.3 Li-ion diffusion in the electrolyte phase

Similarly, in the positive and negative electrodes, the electrolyte concentration is described as:

$$\varepsilon_i \frac{\partial c_e(x,t)}{\partial t} = \frac{\partial}{\partial x}\left[D_{eff,i} \frac{\partial c_e(x,t)}{\partial x} \right] + a_i(1-t_+)\, j(x,t) \tag{7}$$

where $D_{eff,i}$ is the effective electrolyte ionic diffusivity; t_+ is transference number; ε_i is the porosities.

The initial and boundary conditions are presented by imposing zero-flux boundary, i.e.,

$$\left.\frac{\partial c_e}{\partial x}\right|_{x=x_0,x_n} = 0 \tag{8}$$

At the separator interface, the continuity of electrolyte concentration and fluxes should satisfy

$$c_e(x,t)\big|_{x=x_p^-} = c_e(x,t)\big|_{x=x_p^+} \tag{9}$$

$$c_e(x,t)\big|_{x=x_s^-} = c_e(x,t)\big|_{x=x_s^+} \tag{10}$$

$$-D_{eff,p}\left.\frac{\partial c_e(x,t)}{\partial x}\right|_{x=\hat{x}_p^-} = -D_{eff,s}\left.\frac{\partial c_e(x,t)}{\partial x}\right|_{x=\hat{x}_p^+} \tag{11}$$

$$-D_{eff,s}\left.\frac{\partial c_e(x,t)}{\partial x}\right|_{x=\hat{x}_s^-} = -D_{eff,n}\left.\frac{\partial c_e(x,t)}{\partial x}\right|_{x=\hat{x}_n^+} \tag{12}$$

2.4 Potential equation in the electrolyte phase

According to Ohm's law, the potential distributions in the electrolyte phase Φ_e is

$$a_i F j(x,t) = -\frac{\partial}{\partial x}\left(\kappa_{eff,i}\frac{\partial \Phi_e(x,t)}{\partial x} \right) + \frac{\partial}{\partial x}\left(\kappa_{eff,i}\Upsilon T(x,t)\frac{\partial \ln c_e(x,t)}{\partial x} \right) \tag{13}$$

And the boundary conditions are

$$\left.\frac{\partial \Phi_e}{\partial x}\right|_{x=x_0} = 0, \Phi_e\big|_{x=x_n} = 0 \tag{14}$$

At the separator interfaces, similar to the electrolyte concentration, the continuity of the potential and fluxes should satisfy

$$\Phi_e(x,t)\big|_{x=x_p^-} = \Phi_e(x,t)\big|_{x=x_p^+} \tag{15}$$

$$\Phi_e(x,t)\big|_{x=x_s^-} = \Phi_e(x,t)\big|_{x=x_s^+} \tag{16}$$

$$-\kappa_{eff,p}\left.\frac{\partial \Phi_e(x,t)}{\partial x}\right|_{x=x_p^-} = -\kappa_{eff,s}\left.\frac{\partial \Phi_e(x,t)}{\partial x}\right|_{x=x_p^+} \tag{17}$$

$$-\kappa_{eff,s}\left.\frac{\partial \Phi_e(x,t)}{\partial x}\right|_{x=x_s^-} = -\kappa_{eff,n}\left.\frac{\partial \Phi_e(x,t)}{\partial x}\right|_{x=x_s^+} \tag{18}$$

where κ_{eff} represents electrolyte conductivities.

2.5 Temperature

Temperature variations are described through the thermal dynamics including ohmic generation rates $Q_{ohm,p}$, reversible generation rates $Q_{rev,p}$, and reaction generation rates $Q_{rxn,p}$. Their relationship obeys

Copyright © 2021 ICAE

$$\rho_i C_{p,i} \frac{\partial T(x,t)}{\partial t} = \frac{\partial}{\partial x}\left[\lambda_i \frac{\partial T(x,t)}{\partial x}\right] + Q_{rxn,p} + Q_{rev,p} + Q_{ohm,p} \quad (19)$$

where $Q_{ohm,p}$ is the heat generated by the movement of lithium-ions in the solid/liquid; $Q_{rxn,p}$ accounts for the heat generated from ionic flux and over-potentials; and $Q_{rev,p}$ is the heat rise caused by the entropy change [16]; ρ_i is the density.

Boundary conditions considering the continuity of solution and continuity of flux are [17]:

$$-\lambda_p \frac{\partial T(x,t)}{\partial x}\bigg|_{x=x_p^-} = -\lambda_s \frac{\partial T(x,t)}{\partial x}\bigg|_{x=x_p^+} \quad (20)$$

$$T(x,t)\big|_{x=x_p^-} = T(x,t)\big|_{x=x_p^+} \quad (21)$$

2.6 Ionic flux

The flux of the Li-ion intercalation/deintercalation reactions at each electrolyte is modeled by the Butler-Volmer kinetics formula,

$$j(x,t) = 2k_{eff,i}\sqrt{c_e(x,t)\left(c_{s,i}^{\max} - c_s^*(x,t)\right)c_s^*(x,t)} \cdot \sinh\left[\frac{0.5F}{RT(x,t)}\eta_i(x,t)\right] \quad (22)$$

where *i* represents *p* and *n* because the ionic flux takes place in only the positive and negative electrodes; η_i is the overpotentials.

$$\eta_i(x,t) = \Phi_s(x,t) - \Phi_e(x,t) - U_i \quad (23)$$

2.7 Separator

Based on the assumption that there is only diffusion (no ionic flux) at the separator, diffusion in the electrolyte phase at the separator is modeled by

$$\varepsilon_i \frac{\partial c_e(x,t)}{\partial t} = \frac{\partial}{\partial x}\left[D_{eff,i}\frac{\partial c_e(x,t)}{\partial x}\right] \quad (24)$$

Likewise, the electrolyte potential (also ignoring the ionic flux) is,

$$0 = -\frac{\partial}{\partial x}\left(\kappa_{eff,i}\frac{\partial \Phi_e(x,t)}{\partial x}\right) + \frac{\partial}{\partial x}\left(\kappa_{eff,i}\Upsilon T(x,t)\frac{\partial \ln c_e(x,t)}{\partial x}\right) \quad (25)$$

2.8 Current Collectors

Owing to the absence of electrolyte and solid particles, the temperature conservation in the current collectors is expressed by

$$\rho_i C_{p,i} \frac{\partial T(x,t)}{\partial t} = \frac{\partial}{\partial x}\left[\lambda_i \frac{\partial T(x,t)}{\partial x}\right] + \frac{I_{app}^2(t)}{\sigma_{eff,i}} \quad (26)$$

According to Newton's law of cooling, Eq. (27) and Eq. (28) are expressed as:

$$-\lambda_a \frac{\partial T(x,t)}{\partial x}\bigg|_{x=0} = h\left(T_{ref} - T(x,t)\right) \quad (27)$$

$$-\lambda_z \frac{\partial T(x,t)}{\partial x}\bigg|_{x=L} = h\left(T(x,t) - T_{ref}\right) \quad (28)$$

where, the heat exchange coefficient, *h*, is proportional to the reciprocal of temperature insulation. The positive and negative current collectors are denoted by *a* and *z*.

2.9 Solving of the PDAEs

In this paper, the finite volume method (FVM) [18] is employed to solve the DAE by discretizing the domains of the independent variables, the time, *t*, and dimension, *x*, and a 1-Dimensional FVM model is built for solving equations. The core of the FVM is the discretization of dimension *x* and pseudo-second-dimension *r*. As illustrated in Fig.2, a structure in the x-direction is developed by dividing the spatial domain into five non-overlapped sub-domains, i.e., *Na*, *Np*, *Ns*, *Nn*, *Nz*, representing the current collector at positive electrode side, positive electrode, splitter, a negative electrode, and current collector at negative electrode side. The interval with a center x_n is $[x_{n-1/2}, x_{n+1/2}]$. The complexity of Li-ion diffusion equation is the main factor influencing computational efficiency. To minimize the computational effort, the two-parameter polynomial approximation [8] is employed in this paper. The P2D model is programmed in MATLAB, and the static parameters and dynamic parameter ranges are selected following ref. [14].

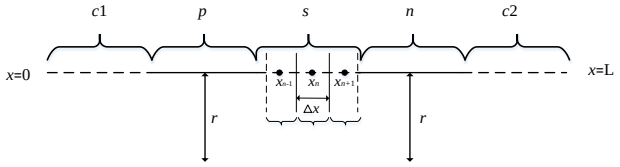

Fig. 2 Model discretization

3. GRADIENT BOOSTING ALGORITHM FOR IMPROVED SOC ESTIMATION

As illustrated in Fig.3, the statistic model is trained with the P2D model producing simulated data to obtain a surrogate model This paper uses the Gradient Boosting Machines (GBMs) model for statistic learning, because GBMs has shown the strong capability of generalization. Then a recurrent model is built to predict the voltage and

Copyright © 2021 ICAE

SOC. The details of the GBMs model are discussed as follows.

$$\eta_m = argmin_\eta \sum_{i=1}^{n} L\left(y_i, f^{(m-1)}(x_i) + \eta s_m(x_i)\right) \tag{32}$$

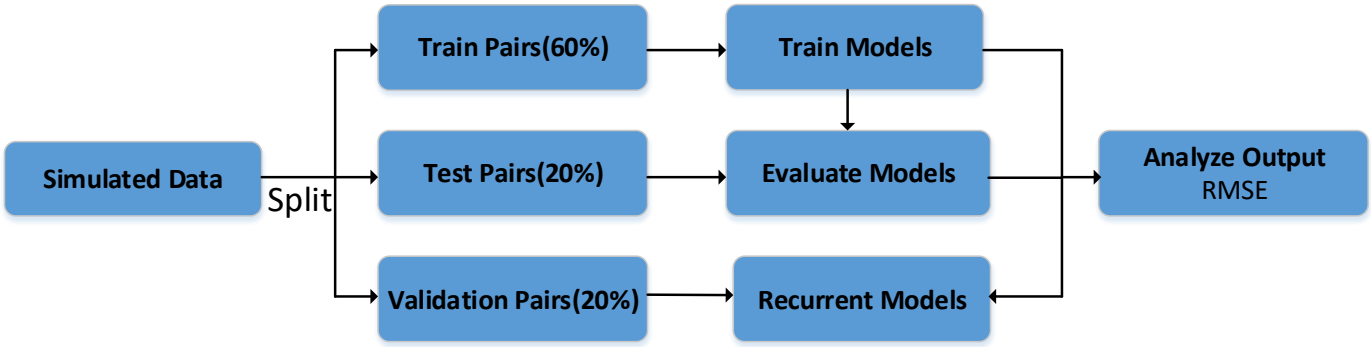

Fig. 3 Process of the surrogate model

3.1 Gradient boosting machines

The GBMs aims to solve a minimization problem defined as

$$(w_m, s_m) = \arg\min_{\{w_m, s_m\}} \sum_{i=1}^{n} L\left(y_i, f^{(m-1)}(x_i) + w_m s_m(x_i)\right) \tag{29}$$

where w_m is a vector of weighting factors for GBM tree; s_m is a list of weak learners of which minimizes the loss function with squared-error [19].

Assuming M decision trees will be constructed, the GBR model is started with an initial model $f^0(x)$, for each iteration $m = 1, 2, \cdots, M$, compensating the residues is equivalent to optimizing the coefficients w_m and s_m.

Since it is hard to find the analytical solution of Eq. (29), this paper utilizes gradient descent to approximate the optimal settings of w_m and s_m. The gradient of the GBMs model can be calculated by

$$-g_m(x) = -\left[\frac{\partial L(y, f(x))}{\partial f(x)}\right]_{f(x)=f^{(m-1)}(x)} \tag{30}$$

where g_m is the negative gradient calculation evaluated using the previous model.

The optimal s_m can be solved using least square formulation,

$$s_m = argmin_s \sum_{i=1}^{n} \left[\left(-g_m(x_i) - s(x_i)\right)\right]^2 \tag{31}$$

The weighting factors of the resulting decision tree, w_m, and the gradient-descent step length μm, are determined by using a line search method; specifically, shrinkage known as learning rate or update rate, which is often used in gradient boosting, is controlled by introducing a new variable μ_m

$$f_m(x) = \mu_m \eta_m s_m(x_i) \tag{33}$$

Ultimately, this proposed problem is solved in the Python package Sci-Kit Learn.

3.2 A recurrent model with the GBMs based surrogate models

In view of the flexibility of machine learning, the typical sets of data are adopted by matching and swapping inputs and outputs. Therefore, sets of training and test data are manipulated by means of time and δ. Previous voltages are used as inputs to predict several next voltages, as described in Eq. (34) and (35). X_{new} and Y_{new} arrays are generated by X_{old} arrays using a set of parameters and previous discharge voltages to predict the next voltage.

$$X_{new}[i] = \left[X_{old}[i, n:n+\delta], Y[i]\right] \tag{34}$$

$$Y_{new}[i] = X_{old}[i, n+\delta+1] \tag{35}$$

To clarify this recurrent process as shown in Fig. 4 δ can be modified to different values. Similarly, the SOC value at each voltage point can be created to predict SOC in such a way.

	Input					Output
n = 0	4.106	4.101	4.097	4.093	4.09	4.086
	4.083	4.089	4.078	4.075	4.075	4.075
				Input		
n = 1	4.106	4.101	4.097	4.093	4.09	4.086
	4.083	4.089	4.078	4.075	4.075	4.075
	Output					

Fig. 4 The generation of recurrent data when δ=5

3.3 Dataset and model learning

In this work, as described in Fig. 5, the simulated data from P2D model is partitioned into three sub-groups,

Copyright © 2021 ICAE

60% for training, 20% for testing, and 20% for validation. The data is collected from 1800 individual discharging tests. The vectors of voltages are disassembled at first and then reassembled such that the input values include a list of parameters and δ voltages, and the output value is the next voltage or next SOC. The range of dynamic parameters, including conductivity of electrodes, diffusion coefficient, reaction rate, and Li+ transference numbers, is obtained in [9].

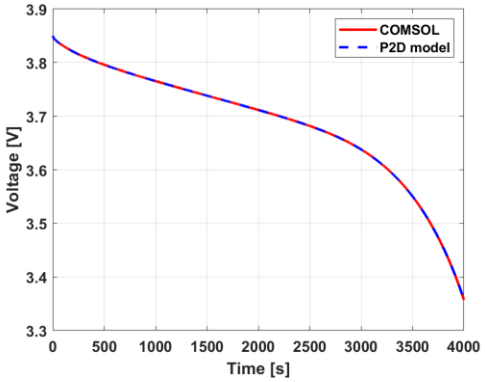

(a)

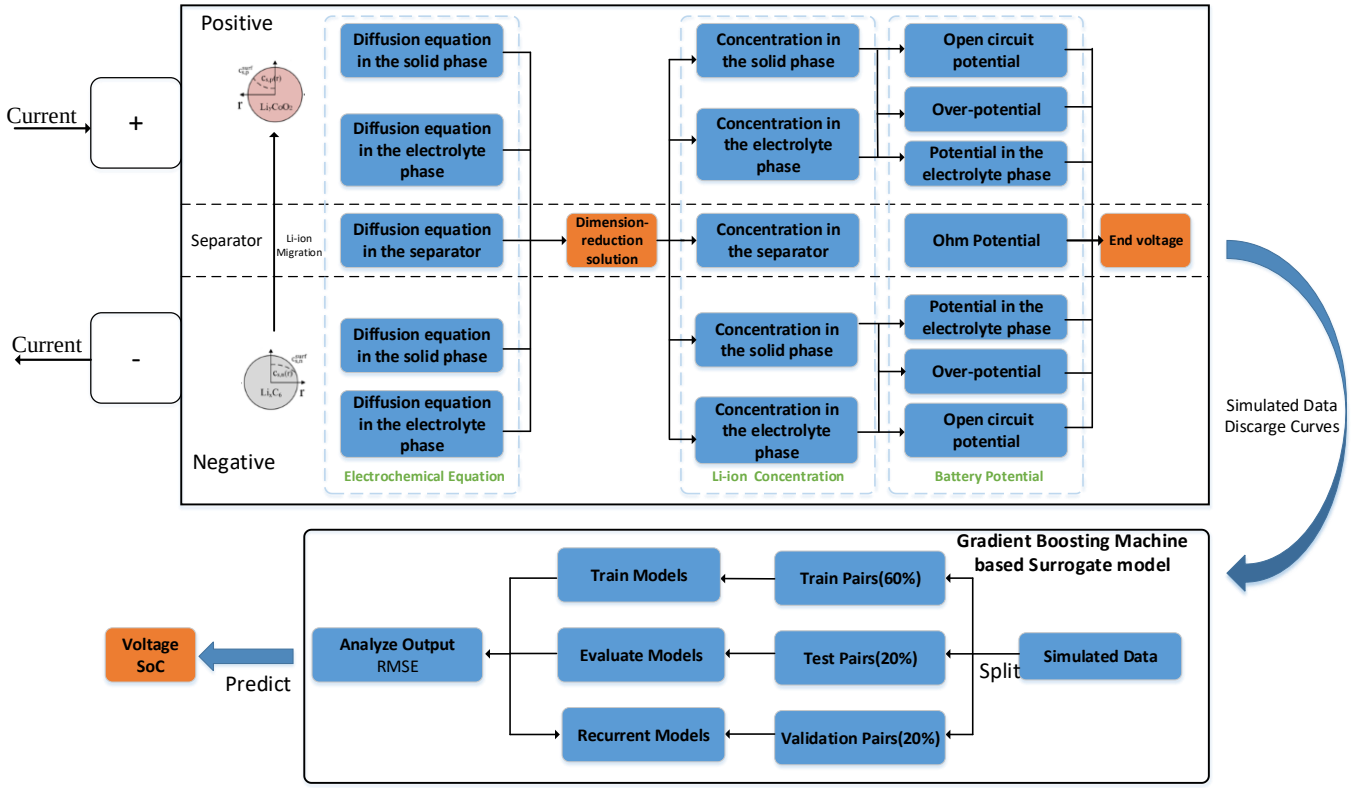

Fig. 5 Prediction and surrogate model

4. RESULTS AND DISCUSSION

4.1 Comparison with the benchmark simulation tool

To validate the numerical calculation of P2D model with thermal dynamics, a comparison study is conducted by using the commercial battery modeling software COMSOL Multiphysics as the benchmark. The battery performance, including voltage, temperature, and solid-phase Li-ion concentration, simulated from the two modeling methods are compared in Fig. 6.

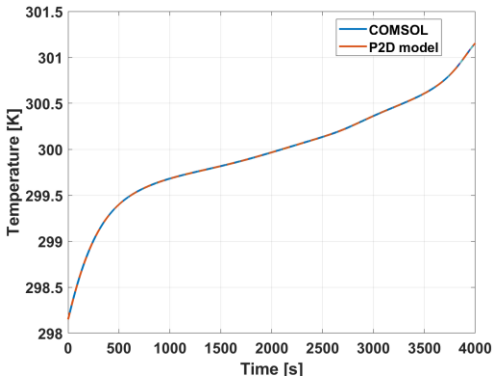

(b)

Copyright © 2021 ICAE

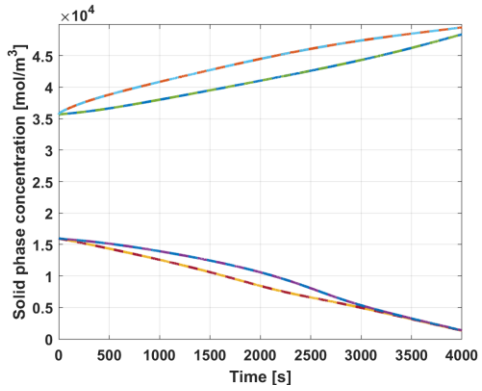

(c)

Fig.6 Validation results (a) Cell Voltage ;(b) Temperature;(c) Solid phase Li-ion concentration

As shown in Fig. 6, the cell voltage, temperature, and other internal states for P2D model are nearly identical to COMSOL.

Table I compares the Root Mean Square Errors (RMSEs) under different cycles. RMSE is high in 10C discharging due to the simplification of the solid-phase diffusion model.

Table I Comparison of RMSEs under different discharging conditions

C rate	RMSE
0.1C	0.052
1C	0.093
5C	0.225

4.2 First Scenario—constant discharge cycles

With the heat exchange coefficient *h* fixed in 1W/(m2K), the voltage and temperature of the battery under constant current discharging are simulated by the proposed P2D model. The results obtained at 0.5C, 1C, and 2C discharging conditions are compared in Fig. 7. It indicates that the temperature increases during the discharging; the high rising rate of the temperature under 2C discharge mainly accounts for the electrolyte concentration being driven to zero in the positive electrode due to the high discharge rate.

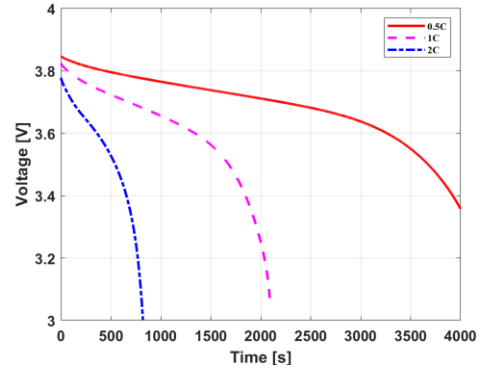

(a)

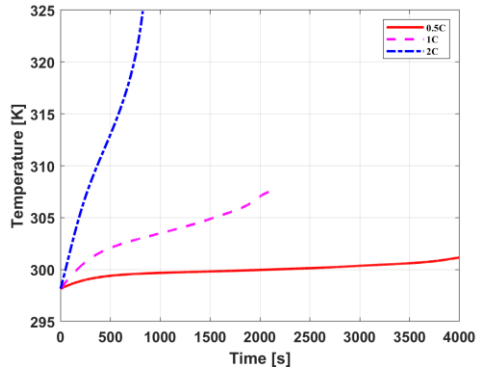

(b)

Fig. 7 Full discharge cycle under different C rates (0.5C/1C/2C) (a)Voltage comparison;(b) Temperature comparison

4.3 Second Scenario—heat exchange coefficient

Different heat exchange coefficients with constant 1C discharge are compared and the results are shown in Fig. 8. The high heat exchange coefficient has the most challenging impact on the dynamic simulations. As expected in Fig. 8, decreasing the value of the heat exchange coefficients h leads to a faster increase of the cell temperature with 0.01W/(m2K)).

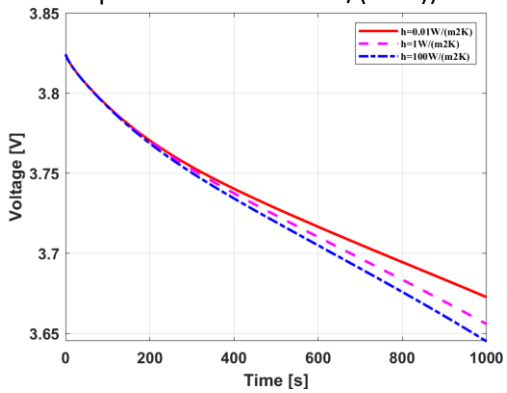

(a)

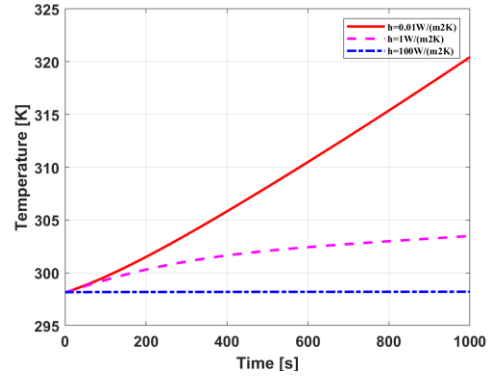

(b)

Fig. 8 1C discharge cycle under different heat exchange parameters (0.01/1/100W/(m2K)) (a)Voltage comparison;(b) Temperature comparison

Copyright © 2021 ICAE

4.4 Third Scenario—charge-discharge cycle

Charge-discharge cycle is designed to simulate a real scene, the battery is charged during braking and discharged during driving, as shown in Fig. 9. In this case, the different C rates in Table I with charge-discharge cycle are mainly responsible for the cell voltage variety with discontinuous changes producing voltage sudden drops. The temperature rises at first, followed by a decrease mainly due to the lower current density applied and heat exchange with the environment.

Table II Charging-discharging simulation

Time	C rate
0-50	-1C
50-100	0.5C
100-250	-0.5C
250-450	-1C
450-460	-2C
460-660	-1C
660-665	0.5C

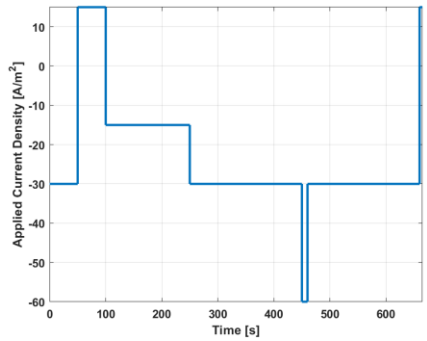

(a)

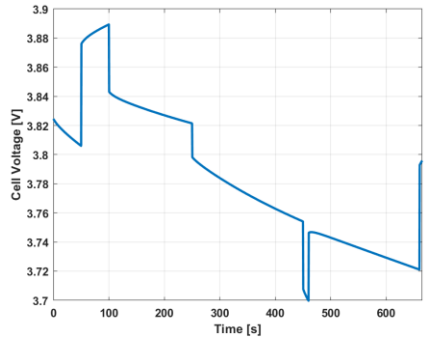

(b)

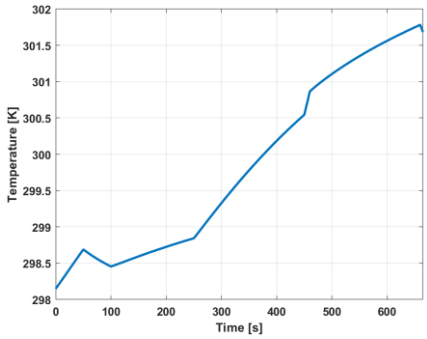

(c)

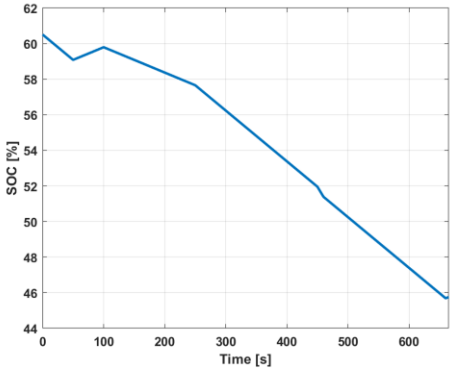

(d)

Fig. 9. Charging-Discharging cycle (a) Current density; (b)Cell voltage; (c)Temperature; (d)SOC

4.5 Voltage Prediction

It is a challenge for a real-time and closed loop control system to employ many sets of complicated equations based on the physical model. Thus, the model is established by using previous voltages to predict the next point including voltages at a fixed interval, combined with different importance on different previous data history.

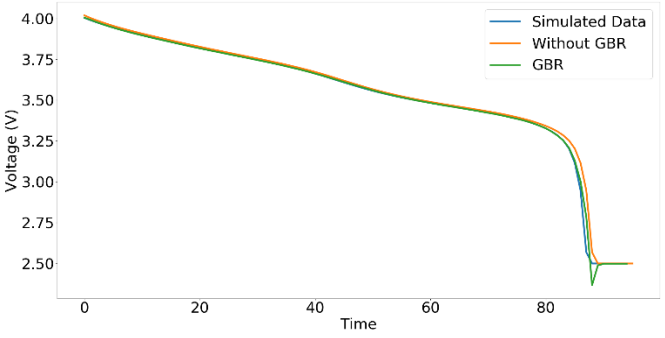

Fig. 10 Gradient-boosted regression voltage prediction by using 5 previous voltages

As shown in Fig. 10, the results from GBMs RMSE of 0.0387 are close to the training data without GBMs of RMSE 0.0258.

4.6 SOC Prediction

Based on the control methods and voltage prediction, it is desirable to obtain SOC estimates for current points or future points or both. The relationship between SoC and voltage at the constant current in Fig. 11, is obtained by the corresponding previous voltage weight to predict the current SOC value in simulation.

Copyright © 2021 ICAE

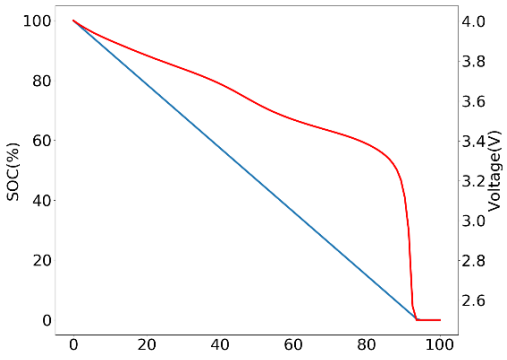

Fig. 11 SoC and voltage at the constant current

5. CONCLUSIONS

In this work, the pseudo-two-dimensional (P2D) model has been discussed and analyzed, taking into account the efficiency and accuracy. A simplification method for modelling and computation has been proposed to shorten simulation time. Then a recurrent model has been established by employing gradient boosting machines to predict voltage and SOC. The research has demonstrated that the surrogate model through the statistical learning could be created to predict the dynamic behavior of the physics-based model. The conclusions are generalized as follows:

1. The simulation results show that the cell voltage, temperature, and other internal states in P2D modeling are nearly identical to those in COMSOL and the physical behaviors are similar in the two models.

2. The training and recurrent models of voltage prediction are effective and the results from GBMs RMSE of 0.0387 are close to training data without GBMs of RMSE 0.0258; this is useful because the corresponding previous voltage weight predicting the current SOC can be used to obtain the linear SOC curves.

3. Since machine learning allows formulation of models using input from the same data set, an interesting future work subject is development of accurate online SOC estimation and prediction models based on historical state data of the battery.

ACKNOWLEDGEMENT

The authors are grateful to the Innovate UK (Grant 102253).

REFERENCE

[1] M. Hua, G. Chen, B. Zhang, and Y. Huang. A hierarchical energy efficiency optimization control strategy for distributed drive electric vehicles, *Proc. Inst. Mech. Eng. Part D J. Automob. Eng.*, vol. 233, no. 3, pp. 605–621, 2019, doi: 10.1177/0954407017751788.

[2] G. Chen, M. Hua, C. Zong, B. Zhang, and Y. Huang, Comprehensive chassis control strategy of FWIC-EV based on sliding mode control, *IET Intell. Transp. Syst.*, vol. 13, no. 4, pp. 703–713, 2019, doi: 10.1049/iet-its.2018.5089.

[3] M. F. M. Sabri, K. A. Danapalasingam, and M. F. Rahmat, A review on hybrid electric vehicles architecture and energy management strategies, *Renew. Sustain. Energy Rev.*, vol. 53, pp. 1433–1442, 2016, doi: 10.1016/j.rser.2015.09.036.

[4] B. Shuai *et al.*, Heuristic action execution for energy efficient charge-sustaining control of connected hybrid vehicles with model-free double Q-learning, *Appl. Energy*, vol. 267, no. November 2019, 2020, doi: 10.1016/j.apenergy.2020.114900.

[5] Q. Zhou *et al.*, Multi-step reinforcement learning for model-free predictive energy management of an electrified off-highway vehicle, *Appl. Energy*, vol. 255, no. June, 2019, doi: 10.1016/j.apenergy.2019.113755.

[6] Q. Zhou, D. Zhao, B. Shuai, Y. Li, H. Williams, and H. Xu, Knowledge Implementation and Transfer With an Adaptive Learning Network for Real-Time Power Management of the Plug-in Hybrid Vehicle, *IEEE Trans. Neural Networks Learn. Syst.*, no. July, 2021, doi: 10.1109/TNNLS.2021.3093429.

[7] A. Jokar, B. Rajabloo, M. Désilets, and M. Lacroix, Review of simplified Pseudo-two-Dimensional models of lithium-ion batteries, *J. Power Sources*, vol. 327, pp. 44–55, 2016, doi: 10.1016/j.jpowsour.2016.07.036.

[8] P. Studies, A Fast Solver for the Pseudo-two-dimensional Model of Lithium-ion Batteries, no. September, 2021.

[9] Y. Zhou, B. C. Wang, H. X. Li, H. D. Yang, and Z. Liu, A Surrogate-Assisted Teaching-Learning-Based Optimization for Parameter Identification of the Battery Model, *IEEE Trans. Ind. Informatics*, vol. 17, no. 9, pp. 5909–5918, 2021, doi: 10.1109/TII.2020.3038949.

[10] X. Han, M. Ouyang, L. Lu, and J. Li, Simplification of physics-based electrochemical model for lithium ion battery on electric vehicle. Part I: Diffusion simplification and single particle model, *J. Power Sources*, vol. 278, pp. 802–813, 2015, doi: 10.1016/j.jpowsour.2014.12.101.

[11] Z. Wei, J. Zhao, R. Xiong, G. Dong, J. Pou, and K. J. Tseng, Online estimation of power capacity with noise effect attenuation for lithium-ion battery, *IEEE Trans. Ind. Electron.*, vol. 66, no. 7, pp. 5724–5735, 2019, doi: 10.1109/TIE.2018.2878122.

[12] M. S. Hossain Lipu *et al.*, Intelligent algorithms and control strategies for battery management system in electric vehicles: Progress, challenges and future outlook, *J. Clean. Prod.*, vol. 292, 2021, doi: 10.1016/j.jclepro.2021.126044.

[13] Z. Wei, Z. Quan, J. Wu, Y. Li, J. Pou, and H. Zhong, Deep Deterministic Policy Gradient-DRL Enabled Multiphysics-Constrained Fast Charging of Lithium-Ion Battery, *IEEE Trans. Ind. Electron.*, vol. 0046, no. c, 2021, doi: 10.1109/TIE.2021.3070514.

[14] N. Dawson-Elli, S. B. Lee, M. Pathak, K. Mitra, and V. R. Subramanian, Data Science Approaches for Electrochemical Engineers: An Introduction through Surrogate Model Development for Lithium-Ion Batteries, *J. Electrochem. Soc.*,

 Copyright © 2021 ICAE

vol. 165, no. 2, pp. A1–A15, 2018, doi: 10.1149/2.1391714jes.
[15] Q. Zhang and R. E. White, Comparison of approximate solution methods for the solid phase diffusion equation in a porous electrode model, *J. Power Sources*, vol. 165, no. 2, pp. 880–886, 2007, doi: 10.1016/j.jpowsour.2006.12.056.
[16] D. H. Jeon, Numerical modeling of lithium ion battery for predicting thermal behavior in a cylindrical cell, *Curr. Appl. Phys.*, vol. 14, no. 2, pp. 196–205, 2014, doi: 10.1016/j.cap.2013.11.006.
[17] X. R. Kong, B. Wetton, and B. Gopaluni, Assessment of simplifications to a pseudo - 2D electrochemical model of Li-ion batteries, *IFAC-PapersOnLine*, vol. 52, no. 1, pp. 946–951, 2019, doi: 10.1016/j.ifacol.2019.06.184.
[18] P. J. Coelho and J. Gonçalves, Parallelization of the finite volume method for radiation heat transfer, *Int. J. Numer. Methods Heat Fluid Flow*, vol. 9, no. 4, pp. 388–404, 1999, doi: 10.1108/09615539910266576.
[19] F. Yang, D. Wang, F. Xu, Z. Huang, and K. L. Tsui, Lifespan prediction of lithium-ion batteries based on various extracted features and gradient boosting regression tree model, *J. Power Sources*, vol. 476, no. May, p. 228654, 2020, doi: 10.1016/j.jpowsour.2020.228654.

 Copyright © 2021 ICAE